Observational cosmology using characteristic numerical relativity

P. J. van der Walt[1] and N. T. Bishop[1]

[1] *Department of Mathematics, Rhodes University, Grahamstown 6140, South Africa*

The characteristic formalism in numerical relativity, which has been developed to study gravitational waves, and the observer metric approach in observational cosmology both make use of coordinate systems based on null cones. In this paper, these coordinate systems are compared and it is then demonstrated how characteristic numerical relativity can be used to investigate problems in observational cosmology. In a numerical experiment using the characteristic formalism, it is shown how the historical evolution of a LTB universe compares to that of the ΛCDM model given identical observational data on a local observer's past null cone. It is demonstrated that, at an earlier epoch of the LTB model, the observational data would not be consistent with that of the ΛCDM model.

PACS numbers:

I. INTRODUCTION

Provided that General Relativity is valid up to the largest scales, under ideal circumstances, the space-time structure of the Universe can be determined by solving the full set of Einstein field equations (EFEs) using observational data as the boundary conditions. Such an observational approach makes use of minimal assumption and observations as the boundary conditions dictate the outcome of the solution. Because of difficulties in obtaining and interpreting observational data, the conventional approach to cosmology is rather based on parameterized models where a model is assumed and then validated against different sets of observations and constraints. Assuming a homogeneous universe with a non-zero cosmological constant and with suitable adjustments of parameters, predictions using the ΛCDM model show remarkable correlation with observed cosmological parameters. The assumption of homogeneity, which is an integral part of this approach, has the implication that local results from simple models can easily be extrapolated to the whole Universe.

However, doing investigations such as quantifying homogeneity on different scales, testing the verifiability of cosmology [1], validating the Copernican principle [2] and determining the metric of the Universe [3], a more suitable methodology is one where the EFEs are solved using a general metric and boundary conditions derived from observations. Since homogeneity is not assumed, conclusions following from the observational approach are necessarily limited to the causally connected region in the interior of our current past null cone on which observations are located. Since the EFEs are solved in a general form, or at least more general than the ΛCDM model, there are more degrees of freedom and also more required boundary conditions. Sufficiently accurate and complete observations do not currently exist, however, it is anticipated that the next generation of astronomical surveys will begin to provide enough detail to perform observational solutions in spherical symmetry.

Much of the development on observational cosmology was inspired by the seminal paper of Kristian & Sachs [4] published in 1966. In their work, observational data was used to determine a general metric but since they made use of series expansions, it was necessarily restricted to a region close to the observer. The ideas introduced by Kristian & Sachs were the starting point of further developments by Ellis, Stoeger, Maartens and others in their *Observational Cosmology* programme with its initial publication in 1985 [1]. In these developments, observational coordinates, based on the concept introduced by Temple in 1938 [5], were implemented to extend the region investigated by Kristian & Sachs to higher redshifts. Observational coordinates are based on null geodesics on the past null cone (PNC) and are therefore the natural framework on which electromagnetic radiation reaches an observer. Solving the EFEs for cosmology then consists of two problems: firstly, astronomical observations are used to determine the metric on the local PNC and secondly

these form the final values of a characteristic final value (CFVP) problem which determines the historical evolution of the region causally connected to the PNC (i.e. the interior of the PNC). The causally connected region is of fundamental importance since it defines the limits on which cosmological models can be validated from direct observations.

In developments towards exact solutions in observational cosmology, spherical symmetrical solutions are taken as a first step to refine the methods (see for instance [6–8]). Spherical symmetry by itself is not necessarily unrealistic since the Universe does appear to be highly isotropic. The spherical symmetrical inhomogeneous Lemaître-Tolman-Bondi (LTB) model in observational coordinates is therefore an important tool for verifying these developments. The LTB model in its standard form also provides a useful framework to investigate solutions from direct observations. In this approach, observations on the PNC are transformed to cosmological coordinates and then related to the coefficients of the LTB metric (e.g. see [9]). These transformations require numerical solutions to handle observational data and recent work by Lu & Hellaby [10] and McClure & Hellaby [11] developed and refined methods for setting up the local PNC from realistic observations with the intention to be implemented on data obtainable in the next generation of astronomical surveys. It should be noted that the emphasis in observational approaches lies in the fact that the initial (final) conditions are provided by direct observations on the PNC and that the EFEs are implemented in a general form with minimal assumptions.

In numerical relativity (NR) methods to implement general solutions of the EFEs have been well established for strong gravitational scenarios where gravitational waves are expected to be formed. Similar to electromagnetic radiation, gravitational radiation also propagates along null geodesics and null cones also provide a natural frame of reference. In this case, however, it is the future null cone that is of interest in the form of a characteristic initial value problem (CIVP). The characteristic formalism in NR is based on the theoretical developments of Bondi, van der Burg & Metzer [12] and Sachs [13] which were part of the *Gravitational Waves in General Relativity* programme initiated by Bondi in the late 1950s. These developments were of fundamental importance to the understanding of gravitational waves and with the advancement of computational technology, it was recognised that the characteristic formalism holds several computational benefits. Among these are: the fact that the EFEs simplify to ordinary differential equations along characteristics, which are less expensive to compute and the conformal method, developed by Penrose [14], can be used to represent infinity on a finite grid, making modelling asymptotical behaviour possible in full non-linearity. One drawback of a null cone coordinate system is its behaviour around caustics where it can become multi-valued and singular. In astrophysical problems, this problem is usually avoided by combining the characteristic formalism with the Cauchy formalism where the latter is used to solve regions where caustics are expected while the former is used to extract the solution in the far field [15, 16]. Treating caustics directly on the null cone has also been investigated [17] but this approach has not been implemented numerically. A comprehensive overview of characteristic numerical relativity can be found in [18].

In the context of cosmology, the CIVP in NR poses the advantages that cosmological developments can leverage on previous developments in astrophysical problems, the causally connected region of the PNC can be computed using realistic boundary conditions free of constraints and the coordinates are simpler than observational coordinates. The simplicity of the coordinates does however introduce restrictions in that the location where the PNC refocusses, the apparent horizon (AH), becomes multi-valued. The importance of the AH has been emphasised in [19] and [8] and methods to cross this region have been presented in [10], [11] and [20] and similar approaches will probably work for the characteristic formalism as well. Although recognising the importance of the AH, the initial steps taken in the current work will be limited to the region where the characteristic formalism is well behaved while the region where caustics occur will be postponed for future research. Applying the CIVP in NR to observational cosmology has previously been investigated by Bishop & Haines in [21] and the work presented in this paper is a continuation of their work. Recent work by Hellaby & Alfedeel [3] defined an algorithm to implement an approach based on observational coordinates with the intention of a numerical implementation. In their work, considerations were taken into account for passing the AH and some other details not taken into account

in this paper but a numerical implementation of their work has not been presented yet.

The work presented in this paper is about evolution off the null cone i.e. the second part of the observational cosmology problem. We develop a computer code, the input to which is data on the PNC obtainable, in principle, directly from observations. The code uses the EFEs to evolve the model into the past. The code reported here is a first step towards the construction of a general code for observational cosmology, and is limited to the case of spherical symmetry.

The code is used to investigate an issue in cosmology. The standard model of the universe is ΛCDM, but it is well known that the observational data also fits a LTB model. The code is used with data on the PNC generated by the ΛCDM model, and we evolve into the past using the $\Lambda = 0$ EFEs. The result is that we compute the data that would be observed on the PNC at an earlier epoch within the context of the LTB model. We then ask the question: Could this data also be interpreted as being that of some ΛCDM model? The answer is "No", which indicates that, if the universe is LTB, then not only are we at a special position in space, but also that the the present time is special in the history of the universe.

In section II, the CIVP is formulated and related to cosmology. Section III presents the implementation of the code, and section IV describes its verification. The results of running the code with ΛCDM model data are given in section V. The paper ends with a Conclusion, section VI.

II. CHARACTERISTIC FORMALISM

A. Metric and coordinates

The essence of the characteristic formalism is a frame of reference based on outgoing null cones that evolve from values on an initial null cone. The idea is conceptualised in figure 1. G is a timelike geodesic, and u is the proper time on G. Null geodesics emanating from G have constant (u, θ, φ), and near G the angular coordinates θ and φ have the same meaning as in spherical polar coordinates. The coordinate r is the diameter, or area, distance from the cone vertex, which means that the surface area of a shell of constant r is $4\pi r^2$.

A spherically symmetric null cone metric based on the Bondi-Sachs metric is: [1]:

$$ds^2 = -e^{2\beta}\left(1 + \frac{W}{r}\right)du^2 - 2e^{2\beta}dudr + r^2\{d\theta^2 + \sin^2\theta d\varphi^2\}. \tag{1}$$

The hypersurface variables, β and W, represent the deviation from a Minkowskian null cone and the coordinate system is defined such that β and W vanish at the vertex of each null cone i.e.: at $r = 0$, equation (1) reduces to a Minkowskian metric.

Substituting (1) into the EFEs, using the form $R_{ab} = 8\pi(T_{ab} - \frac{1}{2}Tg_{ab})$, with the stress-tensor for a dust-like fluid ($T_{ab} = \rho v_a v_b$ and $T = \rho$), leads to expressions for β and W:

$$\beta_{,r} = 2\pi r\rho(v_1)^2 \tag{2}$$

$$W_{,r} = e^{2\beta} - 1 - 4\pi e^{2\beta}\rho r^2 \tag{3}$$

with the initial conditions inherent to the coordinate definition as $\beta(0) = W(0) = 0$. Further,

[1] The notation used here is based on that of [22] and substituting $W = V - r$ will give the original notation of Bondi in [23].

substituting the dust stress tensor and (1) into the conservation equation, $T^{ab}_{\ ;b} = 0$, it follows that:

$$v_{1,u} = \frac{1}{v_1}\left\{(2v_1v_0 - V_w(v1)^2)\beta_{,r} + (V_w v_1 - v_0)v_{1,r} + \frac{1}{2}(v_1)^2 V_{w,r}\right\} \tag{4}$$

$$\rho_{,u} = \frac{1}{v_1}\left\{\rho\left[V_w\left(\frac{2v_1}{r} + v_{1,r}\right) - \left(\frac{2v_0}{r} + v_{0,r}\right) + V_{w,r}v_1\right] + \rho_{,r}\left(V_w v_1 - v_0\right) - \rho v_{1,u}\right\} \tag{5}$$

with: $V_w = 1 + \dfrac{W}{r}$.

An equation for $v_{0,u}$ is also obtained from this but making use of the normalisation condition, $g^{ab}v_a v_b = -1$, a direct expression for v_0 in terms of v_1, β and W can be written as:

$$v_0 = \frac{1}{2}v_1 V_w + \frac{1}{2}e^{2\beta}v_1^{-1}. \tag{6}$$

Without any cosmological considerations, having the values on the initial null cone for ρ and v_1, equations (2) to (6) forms a hierarchical system that can be solved in the order (2), (3) and (6), then solving equations (4) and (5) evolves the system to the next null cone where the process can be repeated until the domain of calculation has been covered. Since these equations are all dependent on each other an iterative scheme is required for a numerical solution.

B. Cosmological coordinates

In observational cosmology, the observer metric is similar to (1) but allows for a more general treatment of the radial coordinate. Using the notation of [6], the metric is defined as:

$$ds^2 = -A^2(w,y)dw^2 + 2A(w,y)B(w,y)dwdy + C^2(w,y)\{d\theta^2 + \sin^2\theta d\varphi^2\}. \tag{7}$$

With reference to the right hand part of figure 1, the coordinates $x^i = \{w, y, \theta, \varphi\}$ are defined as (see [1] and [6]): w, the proper time coordinate on an observer's world line (C), such that $w = constant$ hypersurfaces are past light cones. The instance w_0 is the current time of a local observer, defining our PNC. y, is a radial coordinate defined as a null geodesic on the past light cone comoving with w. There is some freedom in the in the interpretation of y which includes: an affine parameter, the redshift z and the diameter distance $C(w,y)$. As with the characteristic formalism, θ and φ are the spherical inclination and azimuth angles respectively

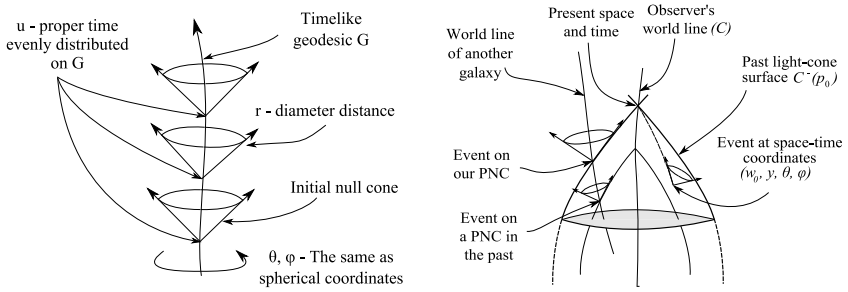

FIG. 1: On the left hand side, the null coordinates of the characteristic formalism and on the right, the null cone coordinates of observational coordinates.

The objective is then to determine $A(w_0, y)$, $B(w_0, y)$ and $C(w_0, y)$ from directly observable quantities and then to solve a CFVP to determine the interior of the null cone. For the spherically

symmetrical dust case observable quantities can be limited to: the redshift z, the apparent luminosity l and number counts n. The redshift (z) is measured in terms of distance related to l and n is obtained in terms of z. These quantities are then related through source evolution functions to the absolute luminosity L and mass per source μ. An important aspect here is that source evolution functions should be model independent [9].

There are three important differences between (1) and (7). Firstly, the characteristic formalism is more restricted in the radial coordinate r which is chosen to be the diameter distance ($r = y = C(w, y)$). This is not a popular choice in cosmology since r will become multi-valued if the null cone starts to refocus at the AH, a situation that can be avoided by making use of y as a distance on the null cone in terms of an affine parameter ν. However, it has been argued in [19] that the position of the AH is an observable property by itself. Knowing this, the model can therefore be adapted to compensate for refocussing possibly in a similar approach to that used in [10]. The details of such a development for the null cone will however not be considered in the current paper and the calculations will be limited to that region of the PNC interior to the refocussing horizon. A second aspect of r is that it is not comoving *viz.* $v^1 \neq 0$. The third difference is that the direction of the null cone is to the future. Changing the direction of the null cone is straightforward by recognising that on a radial null geodesic ($ds = d\theta = d\varphi = 0$ and $du \neq 0$) from the metric (1):

$$\int_{r_1}^{r} dr = -\frac{1}{2}\int_{u_1}^{u}\left(1+\frac{W}{r}\right)du = \frac{1}{2}\int_{u}^{u_1}\left(1+\frac{W}{r}\right)du. \tag{8}$$

Therefore changing the direction of numerical integration can be used to determine the PNC instead of a future null cone.

C. Cosmological observations

The observational properties on the initial PNC as derived by Bishop and Haines [21] will be presented in a modified form to separate the redshift z and the diameter distance r_0. The redshift in terms of the luminosity distance (d_L) is taken to be directly observable to a sufficiently accurate order in the region where the null cone CIVP is well behaved. The reciprocity theorem is used to find a relation between z and r_0 (see [24])

$$z(d_L) \quad \text{and} \quad d_L = (1+z)^2 r_0 \Rightarrow \hat{z} = z(r_0). \tag{9}$$

The redshift is directly related to the time component of the contravariant velocity:

$$1 + \hat{z} = v^0 \tag{10}$$

which can be used to determine the covariant velocity v_1:

$$v_1(u_0, r) = -e^{2\beta}v^0 = -e^{2\beta}(1+\hat{z}). \tag{11}$$

The observed number count (n) is a directly measurable function of z and to be used as input to the CIVP once it has been related to the proper density ρ. Since $\hat{z}(r_0)$ is known, $n(z)$ can be rewritten as $\hat{n}(r_0) = n(\hat{z}(r_0))$. It was shown in [21] that the proper number count can be written as:

$$N = \frac{n}{(1+z)}e^{-2\beta}. \tag{12}$$

In terms of the diameter distance, the proper number count can be written as:

$$\hat{N}(r_0) = \frac{\hat{n}}{(1+\hat{z})}e^{-2\beta}. \tag{13}$$

The proper density is then related to the proper number count:

$$\rho(u_0, r_0) = f(\hat{N}). \tag{14}$$

The details of this relation will not be considered at this stage but in principle it must take into account aspects such as dark matter and source evolution, preferably with factors independent of an already assumed cosmological model.

Solving the CIVP from observational quantities, as with the observer coordinate method, requires that the values on the initial null cone be determined from observational quantities. These values will then be used as the initial values for the evolution into the local past null cone. The solution on the initial null cone follows from equations (11) and (14) but they are dependent on β which is still unknown. Using equations (2), (11) and (14), a differential equation for β which is only dependent on observational quantities for the initial null cone can be set up as:

$$\beta_{,r} = 2\pi r f(\hat{N})(-e^{2\beta}(1+\hat{z}))^2. \tag{15}$$

This equation can be solved numerically with standard ODE techniques provided that $f(\hat{N})$ is well behaved.

III. NUMERICAL IMPLEMENTATION

A. Code outline

The code described in this section is based on the general 3D code developed in [22] and [25] but significantly simplified for spherical symmetry. The numerical scheme applied is a combination of second order finite difference methods based on steps half way between the r and u grid points on a regular grid. The objective has been to obtain overall second order convergence in both space and time up to a distance reasonably close to the location where refocussing will occur.

The procedure described here, is to solve equations (2-6) on a rectangular grid, which is described in more detail in section III B. Solving the hypersurface equations is done with a central difference method on half steps between the r-grid points, using:

$$g^i_j = g^i_{j-1} + \frac{\Delta r}{2}(g^i_{,r\ j} + g^i_{,r\ j-1}) \tag{16}$$

with i being the time step and j the radial step. Here $g^i_{,r\ j}$ is calculated by substituting known values into equations (2) and (3). In order to solve the evolution equations, (4) and (5), their general form is notated as:

$$v_{1,u} = F_{v1} \quad \text{and} \quad \rho_{,u} = F_\rho \tag{17}$$

and as explicit finite differences on a time half step they are written as:

$$v^{n+1}_{1j} = v^n_{1j} + \Delta u F^{n+1/2}_{v1\ j} \quad \text{and} \quad \rho^{n+1}_j = \rho^n_j + \Delta u F^{n+1/2}_{\rho j}. \tag{18}$$

Here, n is a time iterator that will approach i. In these equations, the numerical values at the point (i, j) are used to evaluate the matter terms while the hypersurface derivatives are obtained by substituting the point values directly into the numerical forms of equations (2) and (3). Radial matter derivatives are calculated making use of standard central difference formulae (see for instance [26] p.160-161).

After setting up a suitable grid (as described in section III B), the numerical algorithm can be summarised in the following steps:

i. Set the ρ and v_1 initial values on to the initial grid points. These values will, in principle, be obtained from observations.

ii. Calculate β, W and v_0 from ρ and v_1 on the initial null cone.

iii. Calculate F_j^1 the from the values of v_1, ρ , β, W and v_0.

iv. Set $F_j^{n+1/2} = F_j^1$ and calculate v_1 and ρ as an initial approximation that will approach the actual values with subsequent iterations.

v. Use the new values of v_1 and ρ to calculate β, W and v_0 and their radial derivatives.

vi. Calculate $F_j^{n+1/2}$ from values in (v) and again v_1 and ρ.

vii. Test the calculations in vi for accuracy and convergence. If they are sufficiently accurate, move to the next time step, otherwise repeat steps v. and vi. with the new values of v_1 and ρ.

B. Grid and domain of calculation

The domain of calculation is the interior region of the past null cone starting from the present space-time location up to a region approaching the point where the null cone starts to refocus. A rectangular grid is used to represent the null cone as illustrated in figure 2. An important aspect of the code is that, besides the coordinate conditions $\beta(u,0) = W(u,0) = 0$, the evolution scheme is unconstrained on the inner and outer radial boundary i.e. no central or outer conditions will be required on the r coordinates. These boundaries do, however, still require to be treated differently from the interior region.

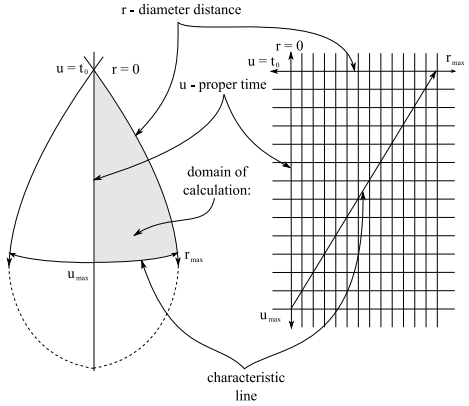

FIG. 2: The past null cone calculated on a rectangular grid

On the central world line ($r = 0$) in figure 2 and its close vicinity, the CIVP equations are not suitable in general form (equations (4) and (5)), which is evident from the occurrence of r denominators. Consequently, the $r \approx 0$ region is calculated by making use of series expansions. In order to do this, all the variables in the CIVP equations are replaced by power series expressions from which the terms can then be calculated from the resulting coefficients. In the expansions, only the terms required to produce second order accuracy will be used, for instance for the density evolution:

$$\rho_{,u} = \rho_{u0} + \rho_{u1} r + \rho_{u2} r^2 + \mathcal{O}(r^3) = F_\rho \, . \tag{19}$$

The region where the series solution meets with the CIVP solution, also requires special treatment to avoid artificial instabilities which has been done by smoothing out the merger region with a weighted average between the two solutions.

In order to evolve the CIVP equations without any boundary condition on the outer radial boundary, the outer boundary must be an incoming null hypersurface. This is needed for well-posedness, and if violated leads to an numerical instability. An incoming null ray (i.e. on a radial null geodesic $ds = d\theta = d\varphi = 0$ and $du \neq 0$) is selected for the outer radial limit and is defined from the metric in the following way:

$$r_{outer} - r_{outer\ u_1} = -\frac{1}{2}\int_{u_1}^{u}\left(1 + \frac{W}{r}\right) du \tag{20}$$

Numerically this can be solved by using an iterative scheme which starts with estimating $W = 0$ and is then repeated until the values of W and r converge. Since the value of r does not necessarily fall directly on grid points, W is determined by linearly interpolating between the closest grid points on a specific u_i grid line. The behaviour of the density evolution is shown in figure 3, where the computation extends beyond the null ray cut-off region in order to illustrate the stability issue.

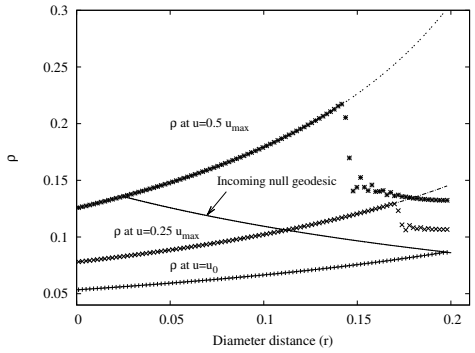

FIG. 3: Unstable regions being excluded using a null geodesic on the outer boundary. The figure is based on a portion of a normalised Einstein-de Sitter calculation.

IV. CODE VERIFICATION

A. LTB models

The spherically symmetric CIVP for cosmology is effectively the Lemaître-Tolman-Bondi (LTB) model in null coordinates. Originating and developed by Lemaître [27], Tolman [28] and Bondi [29], the LTB model is a generalisation of the Friedmann-Lemaître-Robertson-Walker (FLRW) model with inhomogeneities allowed in the radial coordinate. The parabolic case of the LTB model is of interest for the investigations in this paper and will be used to verify the CIVP code. The metric in comoving synchronous coordinates is:

$$ds^2 = -dt^2 + [R_{,r}(t,r)]^2 dr^2 + [R(t,r)]^2\{d\theta^2 + \sin^2\theta d\varphi^2\} \tag{21}$$

Here, t is the cosmic (proper) time, r is a comoving radial coordinate with θ and φ the inclination and azimuth angles. $R(t,r)$ is the areal radius and $4\pi R^2$ defines the proper surface area of a sphere with coordinate radius r at a constant time slice [30]. Substituting into the Einstein field equations and solving gives (see [31]):

$$R(t,r) = \left[\frac{9}{2}M(r)(t - t_B(r))^2\right]^{1/3} \quad \text{and} \quad \rho(t,r) = \frac{M_{,r}}{4\pi\ R^2 R_{,r}}\ . \tag{22}$$

$M(r)$ is the *active gravitational mass* which is the mass contributing to the gravitational field and $t_B(r)$ is defined as the *bang time function*, which is a surface defined by the local time at which $R = 0$.

In order to provide data to verify the CIVP code against known solutions, LTB models need to be transformed to null coordinates which will then be used as input data on the initial null cone as well as comparative data inside the null cone. Numerous LTB models exist which include the FLRW models, other physical realistic models and also many models with uncertain physical relevance. Many physical LTB scenarios have been investigated that are possible candidates of the actual universe (see for instance [32]) which will all be interesting scenarios to run on a CIVP code. However, for the purpose of code verification, it will be conducive to work with models that are mathematically simple, well documented and physically relevant. The class of LTB models that will be investigated is referred to as *bang time models* and makes use of the bang time function, t_B, as a mechanism to induce inhomogeneities into a universe. By selecting simple functions for t_B, it has been demonstrated that inhomogeneities can mimic the effect of inflation (solving the horizon problem) [33, 34], describe the cosmic microwave background (CMB) dipole anisotropy [35], and how inhomogeneities can reproduce the effect of supernovae-redshift dimming without the requirement of dark energy [36].

For these models, $M(r) = M_0 = r^3$ is chosen as a coordinate condition where M_0 is a constant which for illustrative purposes is set to $2/9$. Equations (22) then reduce to:

$$R(t, r) = r(t - t_B(r))^{2/3} \tag{23}$$

with:

$$R_{,r}(t, r) = \frac{t - t_B(r) - 2/3\, r\, t_{B,r}(r)}{(t - t_B(r))^{1/3}} \tag{24}$$

and ρ in equation (22) to:

$$\rho(t, r) = \frac{1}{2\pi(t - t_B(r))(3t - 3t_B(r) - 2rt_{B,r}(r))}. \tag{25}$$

By selecting $t_B(r) = 0$, it can be seen that, equation (25) becomes the Einstein-de Sitter (EdS) model, which has been used as a test compared in previous work [21]. If $t_B(r) \neq 0$ and $t_{B,r}(r) = 0$, the time of the initial singularity is adjusted and the age of the Universe changes. For non-constant functions, the initial singularity becomes a singular surface and the age of the Universe becomes subject to the position of an observer (i.e. the age of the Universe depends on r). Thus, a variety of models can be generated for testing the code on parabolic spatial sections.

B. Coordinate transformations

In order to generate results from LTB models on the null cone, a coordinate transformation must be made from equation (1) to equation (21). For simplicity, the null cone metric will be written in the form:

$$ds^2 = -h_u du^2 - 2h_r du dr + r^2\{d\theta^2 + \sin^2\theta d\varphi^2\}. \tag{26}$$

and the coefficients will be rewritten in terms of W and β afterwards. Also, LTB variables that have the same symbols as the null cone variables will be notated using a tilde e.g. $r_{LTB} = \tilde{r}$, $v_{1\,LTB} = \tilde{v}_1$, $g_{LTB} = \tilde{g}$ etc.

The essence of the transformations is to relate the (u, r) coordinates to corresponding $(t, \tilde{r})$ values. An expression for r in terms of $\tilde{r}$ and t can be obtained by comparing the coefficient of $(d\theta^2 + \sin^2\theta d\varphi)$ in the two coordinate systems, leading to

$$R(t, \tilde{r}) = r \tag{27}$$

A second expression containing u, $\tilde{r}$ and t can be found by making a transformation from LTB coordinates to find in null cone coordinates the term g^{00}, which is equal to zero. A first order partial differential equation follows:

$$0 = \frac{\partial u}{\partial \tilde{r}} - [R_{,\tilde{r}}(t,\tilde{r})]\frac{\partial u}{\partial t} \quad \text{with} \quad u(t,0) = t \tag{28}$$

which, using the method of characteristics, can be written as:

$$\frac{dt}{d\tilde{r}} = -[R_{,\tilde{r}}(t,\tilde{r})]. \tag{29}$$

Depending on the complexity of the $R_{,\tilde{r}}$ term, either numerical or analytic methods can be used to solve this equation.

Expressions containing partial derivatives for the other null cone terms can be obtained from covariant transformations. For h_r and h_u these are:

$$h_r = \frac{\partial t}{\partial u}\frac{\partial t}{\partial r} - [R_{,\tilde{r}}(t,\tilde{r})]^2\frac{\partial \tilde{r}}{\partial u}\frac{\partial \tilde{r}}{\partial r} \tag{30}$$

$$h_u = \left(\frac{\partial t}{\partial u}\right)^2 - [R_{,\tilde{r}}(t,\tilde{r})]^2\left(\frac{\partial \tilde{r}}{\partial u}\right)^2 \tag{31}$$

Having values for h_u and h_r, the Bondi-Sachs coefficients can be obtained from:

$$\beta = \frac{1}{2}\ln \mid h_r \mid \quad \text{and} \quad W = r(h_u h_r - 1)$$

In order to write v_1 in null coordinates, requires the transformation of the comoving velocity ($\tilde{v}^\mu = (1,0,0,0)$ and $\tilde{v}_\mu = (-1,0,0,0)$) into null coordinates.

$$v^0 = \frac{\partial u}{\partial t} \quad , \quad v^1 = \frac{\partial r}{\partial t} \quad , \quad v_0 = -\frac{\partial t}{\partial u} \quad \text{and} \quad v_1 = -\frac{\partial t}{\partial r} \tag{32}$$

The five point difference equations in [26] were used to determine the grid values of equations (30), (31) and (32); v_1 from (32) together with ρ from (25) are used as the input data on the initial null cone.

C. Verification results

A simple choice of bang function is implemented as a verification model:

$$t_B(r) = br, \tag{33}$$

with b being a constant. This simplifies equations (23), (24) and (25) to:

$$R(t,r) = r(t-br)^{2/3} \tag{34}$$

$$R_{,r}(t,r) = -\frac{1}{3}\frac{(-3t+5br)}{(t-br)^{1/3}} \tag{35}$$

$$\rho(t,r) = \frac{1}{2\pi(t-br)(3t-5br))}. \tag{36}$$

The effect of different values of b on the shape of the PNC is shown in figure 4 where different models have been scaled and transposed relative to an observer located at the vertex of the PNC of a normalised EdS universe. The value $b = 0$ is exactly the EdS model and $b > 0$ shifts the

age of a universe to a younger age as r increases while $b < 0$ provides the opposite effect where a universe is shifted to an older age as r increases. The latter case is particularly interesting since it provides a mechanism to mimic a cosmological constant [36]. In figure 4 a reasonable match on the shape of the ΛCDM ($\Omega_\Lambda = 0.7$) PNC is shown by a $b = -0.5$ bang time model before the PNC refocusses. This is however not an exact physical match but provides a useful verification model since the shape of the null cone is a critical aspect on the stability of a CIVP code.

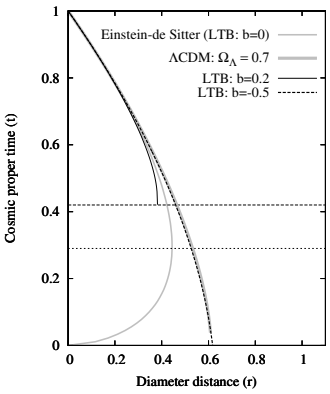

FIG. 4: The past null cone of different bang time models compared to the Einstein-de Sitter model and the ΛCDM model.

The test cases presented in this section are the $b = 0$ (EdS) case up to 0.82 u_{max} and 0.82 r_{max} and the $b = -0.5$ case up to 0.75 u_{max} and 0.8 r_{max} with u_{max} and r_{max} the time and distance of the AH. The EdS case provides a useful baseline since its solution is exactly known in null coordinates while the $b = -0.5$ case is representative of an LTB model with a ΛCDM-like PNC. It should be noted that the EdS model is **not** homeogeneous with respect to the null cone radial coordinate r and is therefore also representative of more general LTB models. The limits chosen are the maximum values where stable solutions were achieved. Extending these limits further causes the code breaks down rapidly, which is the expected behaviour close to the AH.

The radial outer limits of the initial PNCs correspond to observations at $z = 0.47$ and $z = 0.48$ in the EdS and LTB cases respectively. By reducing the extent of u limit, the radial extent can be increased and conversely reducing the radial limit allows the u limit to be increased, for instance values of 0.2 u_{max} and 0.99 r_{max} ($z = 1.02$) also produce stable results for the EdS model. The stability in terms of the radial and evolution limits is dependent on the input data and the simulations in section V were stable up to $z \approx 1$, which is a significant region for supernovae redshift-distance observations. In this section values were chosen that were useful for demonstrating accuracy and stability on normalised models.

1. Physical variables

Figure 5 shows the density (ρ) and covariant velocity (v_1) of the two models. The plots contain lines, which represent the exact values, and points representing the code values. The exact and code values are close enough not to show visible deviations. The density distributions of the two models on the oldest PNC are interesting to compare where the $b = -0.5$ model clearly displays the effect of the bang time surface.

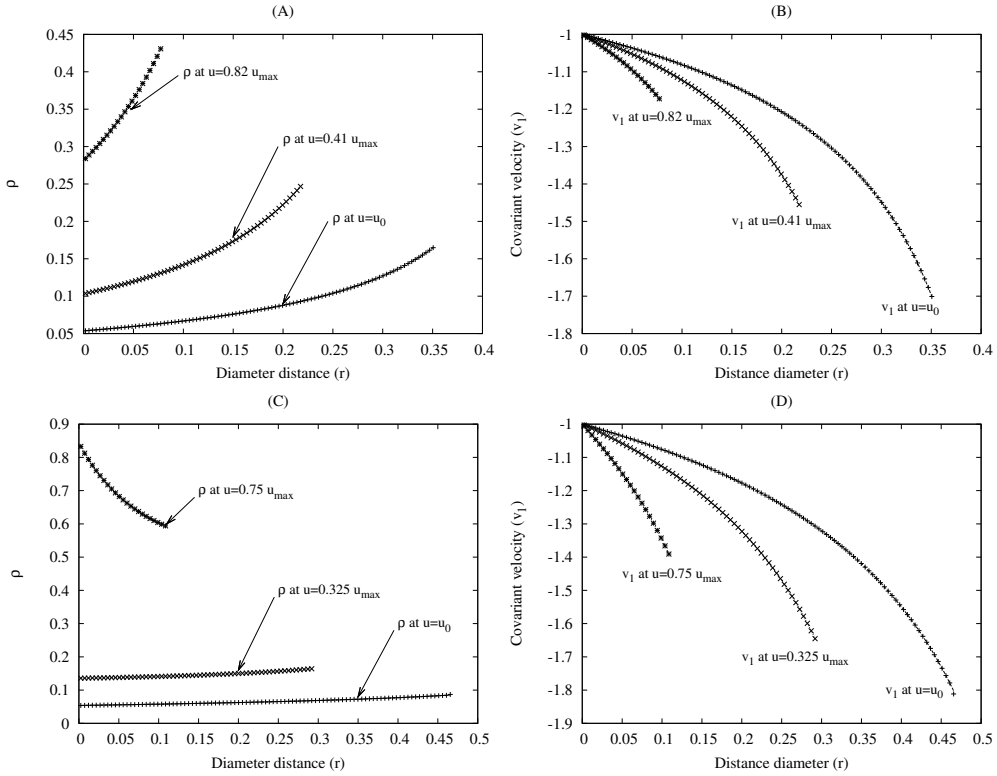

FIG. 5: ρ and v_1 against r on null cones in the past for the Einstein-de Sitter model (A) and (B) and the $b = -0.5$ bang time model (C) and (D).

2. Local error propagation and convergence

Figure 6 shows the radial distributions of the relative errors on the oldest null cones. As a measure of errors, the relative percentage of the difference between the exact and code of the density calculation has been chosen as a representative quantity. This choice has been based on different test cases where small errors in the other variables, v_1, W and β have become pronounced in the density calculation. The EdS model having more accurate input values has a better local accuracy but the series-CIVP merger region is more visible in the $r \approx 0$ region.

In figure 7, errors are shown where grid resolution has been refined three times. It can be seen that errors in the region where the series solution is merged with the CIVP solution is significantly larger at low grid resolutions but converge rapidly to containable levels. The merging region between the series and CIVP solution is particularly sensitive which suggests that further refinement of this region will be required especially if realistic observational data will be used as input in future research.

In figure 8, the convergence against the radial grid size is shown. Here the slope of the line on a log scale is 1.9 and 1.8 for the EdS and $b = -0.5$ cases respectively, indicating that convergence approaches second order. The fact that the code breaks down after being close to second order accurate is as an accuracy consideration a useful feature since it doesn't produce false results; it either works accurately or provides no results.

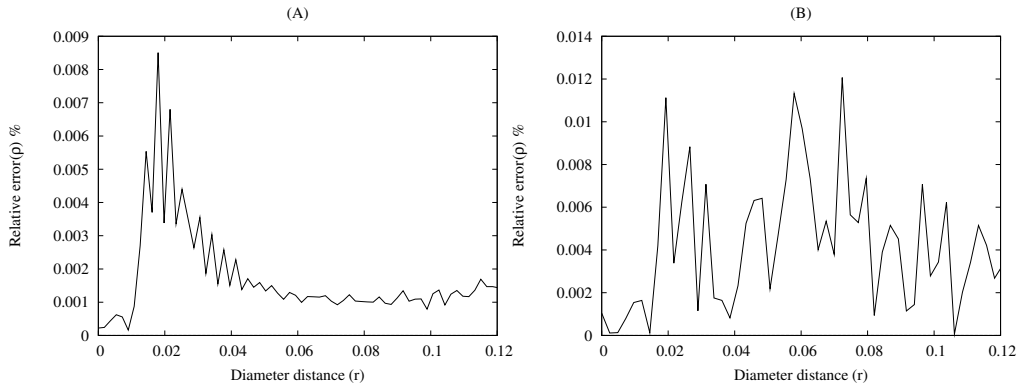

FIG. 6: Spatial error vs. r for 200 r × 1000 u grid points for the Einstein-de Sitter model (A) and the $b = -0.5$ bang time model (B).

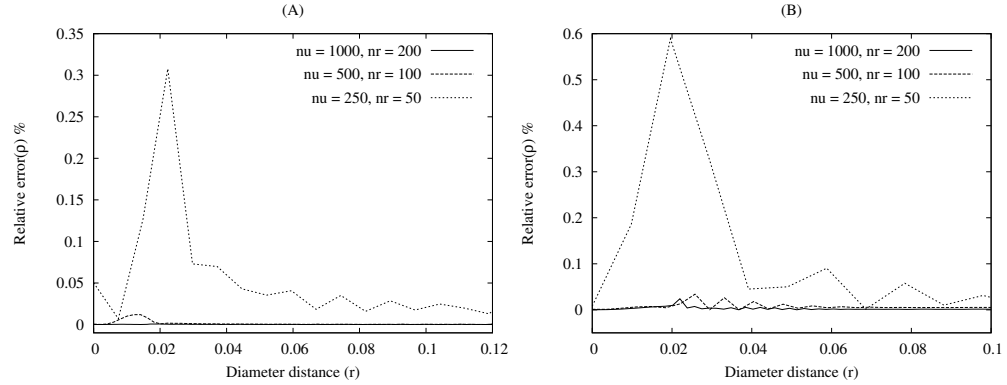

FIG. 7: Grid convergence: The error propagation for $u \times r$ grid resolutions of 1000×200, 500×100 and 250×50 for the Einstein-de Sitter model (A) and the $b = -0.5$ bang time model (B).

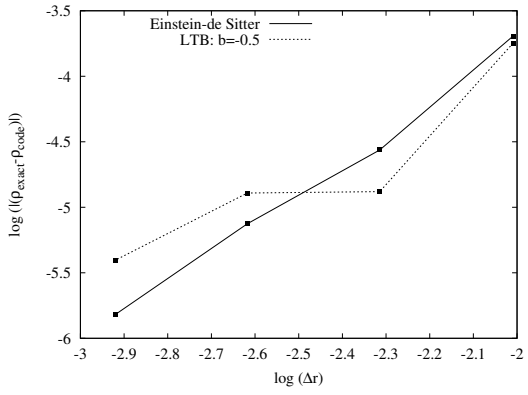

FIG. 8: Grid convergence: The slope of the $\log(error_{max})$ vs. $\log(\Delta r)$ line is 1.9 for a $\Delta r/\Delta u \approx 3.1$ grid for the Einstein-de Sitter model and 1.8 for a $\Delta r/\Delta u \approx 3.2$ grid for the $b = -0.5$ bang time model.

V. LTB VS. ΛCDM

A. Overview

Following from the *Isotropic Observations Theorems* in [9] (also see [30]), any reasonable set of spherical symmetrical observations can be accommodated by some distribution of inhomogeneities in an LTB model. Soon after the discovery of dark energy from Supernovae Ia observations in 1998 [37, 38], using this principle, it was demonstrated by Célérier [36], with others to follow (e.g. [39]), that the same observational effects can be caused by radial inhomogeneities without any need of a cosmological constant. The concept of inhomogeneities mimicking dark energy has been investigated many times since then, mostly as toy models demonstrating the ambiguity of observations commonly accepted in conventional cosmology. The main argument against LTB universes is that they place the observer in the centre of the Universe which, although not impossible is not a philosophically appealing idea. Even so, with a CIVP code at hand, an interesting numerical experiment is to test the historical evolution of an LTB model, with a zero cosmological constant, when observational data representing that of the ΛCDM model is interpreted as being caused by inhomogeneities.

A simple simulation set up for this experiment is done by calculating the density ρ and covariant velocity v_1 on the past null cone by transforming exact solutions for a flat ΛCDM model onto the past null cone. These are then used as input to the code and compared to the transformed model. In terms of the LTB metric (21), using cosmological properties at the current epoch (t_0), the solution of the flat ΛCDM model is (see [40]):

$$R(t,\tilde{r}) = S(t)\,\tilde{r} = \left(\frac{\Omega_{m0}}{\Omega_{\Lambda 0}}\right)^{1/3} \left(\sinh\left[\frac{3}{2}H_0\sqrt{\Omega_{\Lambda 0}}\,t\right]\right)^{2/3} \tilde{r} \tag{37}$$

with the age of the Universe:

$$t_0 = \frac{2}{3}\left(H_0\sqrt{\Omega_{\Lambda 0}}\right)^{-1} \sinh^{-1}\left[\left(\frac{\Omega_{\Lambda 0}}{\Omega_{m0}}\right)^{1/2}\right] \tag{38}$$

and the density distribution

$$\rho_m = \frac{3H_0^2}{8\pi G}\frac{\Omega_{m0}S_0^3}{S^3}. \tag{39}$$

Here, Ω_{m0} and $\Omega_{\Lambda 0}$ are the current density parameters for Baryonic matter and the cosmological constant respectively and H_0 is the current Hubble constant. The values used to represent the actual Universe were: $\Omega_{m0} = 0.3$, $\Omega_{\Lambda 0} = 0.7$ and $H_0 = 72$ Mpc s^{-1} km^{-1}. An important issue to notice here is that ρ_m in the ΛCDM model is determined by parameters related to the expansion and the density content and not by an independent measure of matter distribution such as number counts. The additional degree of freedom introduced in the LTB model is therefore not purely satisfied by an additional boundary condition which is a limitation that should be borne in mind when interpreting redshift dimming as an LTB model.

Figure 9 shows the resulting LTB vs. ΛCDM evolutions back in time. While it might currently not be possible to distinguish these models from one another based on observations on the past null cone, in the past, these universes are distinctly different. In particular, the LTB universe seems to be heading towards a singularity much faster than the ΛCDM universe and would therefore be significantly younger, if the trend is to continue beyond the calculations.

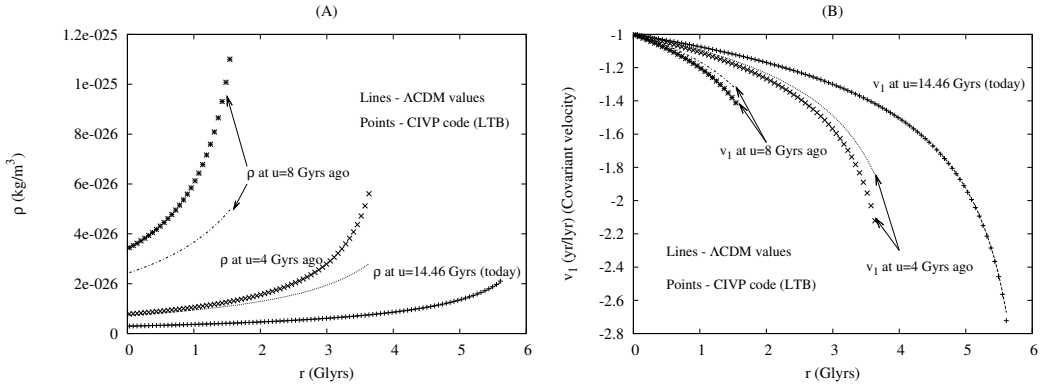

FIG. 9: Density distribution (A) and covariant velocity (B) on past null cones at different proper times (u)

B. LTB vs. ΛCDM matching

A question arising from the results presented in figure 9 is: if the LTB null cones in the past would also represent ΛCDM flat space null cones? In this section an attempt is made to find a matching ΛCDM model for the $t_0 - 8$Gyrs LTB null cone. The procedure followed here is to firstly find a null cone in the past of a selected ΛCDM model for which the density corresponds to the LTB density at $r = 0$. This gives a density curve which has the same starting point but the slope of the curve differs to that of the LTB model. The slope of the curve is then matched by adjusting the Hubble rate (H_0) until it approximately corresponds to the LTB curve. The covariant velocities (v_1 as a function of r) are then compared to see, qualitatively, if the models can be regarded as the same.

The models investigated are summarised in table I and detailed results are shown in the figures 10 to 13. From table I it can be seen that the matching instances are from universes with different ages and matching takes place at different times in their evolutions. From the detailed results, it becomes apparent that matching both the radial matter distribution and expansion through ρ and v_1 is an unlikely proposition. Applying the matching procedure to ρ causes v_1 to move away from the ΛCDM data while ρ moves away when v_1 is matched. This then suggests that the past null cones do not represent a ΛCDM model. This is an illustration of similar conclusions found by Yoo, Kai & Nakao [20].

An interesting correlation is that the values of H_0 and t_{match} are very close for all the models and it might be possible that they are in fact the same. A formal correlation was however not done since the qualitative behaviour of the covariant velocities rules out a reasonable match in any of the models. The plots are presented in figures (10) to (13) which reveal a surprising similarity in the v_1 plots.

VI. CONCLUSION

In this paper we demonstrated how to use the characteristic formalism of numerical relativity to investigate problems in observational cosmology. For this purpose, a CIVP code was developed and it was shown that the code is second order accurate and stable for selected LTB models in the

Ω_Λ	H_0 (Mpc s^{-1} km^{-1})	Age (t_0) (Gyrs)	Density matching time (t_{match}) (Gyrs)	Figure
0	86	8.34	4.44	10
0.5	84	10.66	4.48	11
0.7	84	12.36	4.45	12
0.9	84	16.39	4.43	13

TABLE I: ΛCDM models used to match the LTB density profile.

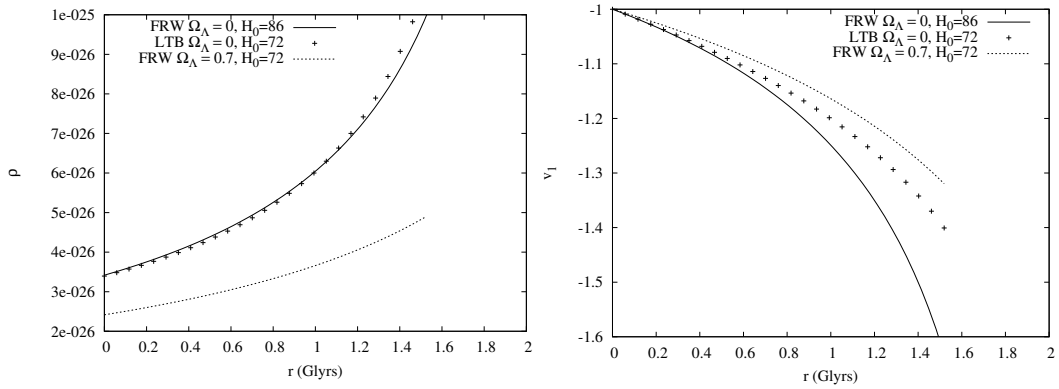

FIG. 10: Density distribution and covariant velocity on the past null cones: LTB with $\Omega_\Lambda = 0$ and FLRW with $\Omega_\Lambda = 0.7$ at $t_0 - 8$Gyrs and the best fit FLRW $\Omega_\Lambda = 0$ instance.

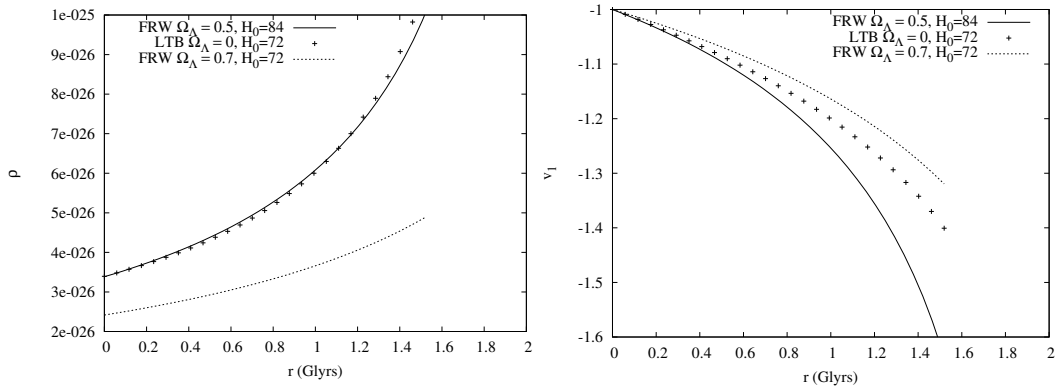

FIG. 11: Density distribution and covariant velocity on the past null cones: LTB with $\Omega_\Lambda = 0$ and FLRW with $\Omega_\Lambda = 0.7$ at $t_0 - 8$Gyrs and the best fit FLRW $\Omega_\Lambda = 0.5$ instance.

region before the PNC starts to refocus. By doing a numerical experiment with LTB vs. ΛCDM data, it was demonstrated that although the initial values of the two models can correspond on the current past null cone, the histories of the two models are distinctly different. The density of the LTB model rises significantly more quickly indicating a much younger universe, possibly too young. The result that past null cones evolved from an initial LTB null cone cannot be matched with a flat ΛCDM model has an important implication: While in our current epoch the LTB vs. ΛCDM ambiguity is difficult to disentangle, this is a feature of the Universe's current state and not its past. *In other words, if the Universe is inhomogeneous without a cosmological constant, not only is the observer in a privileged position (near a central point), he also lives in a specific time where the Universe can appear to be either LTB or ΛCDM.* It would be interesting to investigate extending this result to non-flat models.

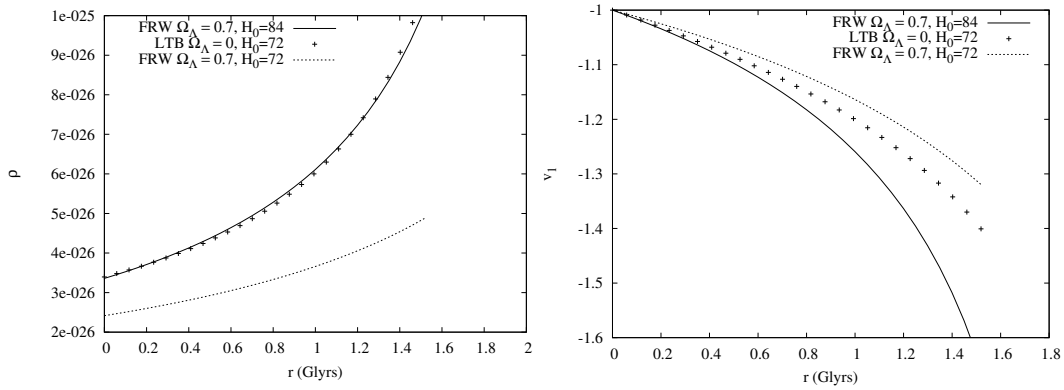

FIG. 12: Density distribution and covariant velocity on the past null cones: LTB with $\Omega_\Lambda = 0$ and FLRW with $\Omega_\Lambda = 0.7$ at $t_0 - 8$Gyrs and the best fit FLRW $\Omega_\Lambda = 0.7$ instance.

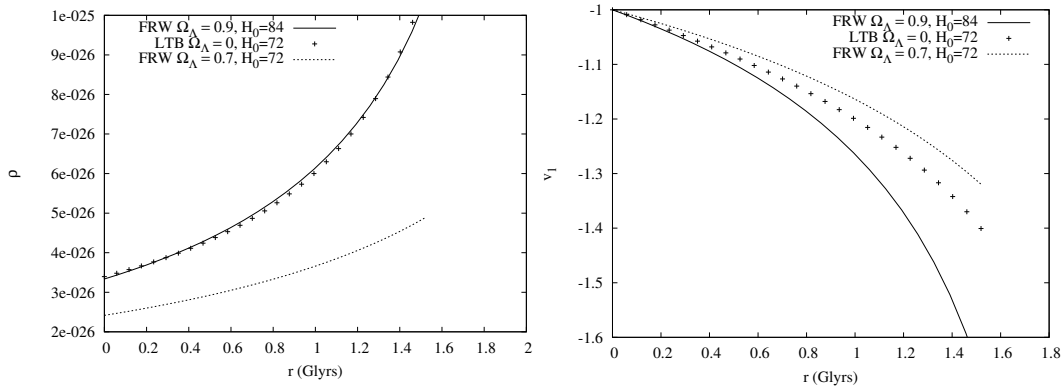

FIG. 13: Density distribution and covariant velocity on the past null cones: LTB with $\Omega_\Lambda = 0$ and FLRW with $\Omega_\Lambda = 0.7$ at $t_0 - 8$Gyrs and the best fit FLRW $\Omega_\Lambda = 0.9$ instance.

Acknowledgments

This work was supported by the National Research Foundation, South Africa.

[1] G.F.R. Ellis, S.D. Nel, W.J. Stoeger, Maartens R., and A.P. Whitman. Ideal observational cosmology. *Phys. Reports*, 124:315–417, 1985.

[2] J. Uzan and G.F.R Ellis. Time drift of cosmological redshifts as a test of the copernican principle. *Phys. Rev. D*, 100:191303–1–191303–4, 2008.

[3] H. Hellaby and A.H.A. Alfedeel. Solving the observer metric. *Phys. Rev. D*, 79:043501–1–043501–10, 2009.

[4] J. Kristian and R.K. Sachs. Observations in Cosmology. *Astrophys. J.*, 143:379–399, 1966.

[5] G. Temple. New Systems of Normal Co-ordinates for Relativistic Optics. *Proc. R. Soc. Lond. A*, 168(932):122–148, 1938.

[6] W.R. Stoeger, G.F.R. Ellis, and S.D. Nel. Observational cosmology: III. Exact spherically symmetric dust solutions. *Class. Quantum Grav.*, 9:509–525, 1992.

[7] M.E. Araújo and W.R. Stoeger. Exact spherically symmetric dust solution of the field equations in observational coordinates with cosmological data functions. *Phys. Rev. D*, 60:104020–1–104020–7,

2000.

[8] M.E. Araújo and W.R. Stoeger. Obtaining the time evolution for spherically symmetric lemaitre-tolman-bondi models given data on our past light cone. *Phys. Rev. D*, 80:123517–1–123517–9, 2009.

[9] N Mustapha, C. Hellaby, and G.F.R Ellis. Large scale inhomogeneity vs source evolution: Can we distinguish them? *Mon. Not. Roy. Ast. Soc.*, 292:817–830, 1998.

[10] T. H.-C. Lu and C. Hellaby. Obtaining the spacetime metric from cosmological observations. *Class. Quantum Grav.*, 24:4107–4131, 2007.

[11] M.L. McClure and C. Hellaby. Determining the metric of the Cosmos: Stability, accuracy, and consistency. *Phys. Rev. D*, 78:044005–1–044005–17, 2009.

[12] H. Bondi, M.G.J. van den Burg, and A.W.K. Metzner. Gravitational Waves in General Relativity. VII. Waves from Axi-symmetric Isolated Systems. *Proc. R. Soc. Lond. A*, 269:21–52, 1962.

[13] R.K. Sachs. Gravitational Waves in General Relativity. VIII. Waves in Asymtotically Flat Space-Time. *Proc. R. Soc. Lond. A*, 270:103–126, 1962.

[14] R. Penrose. Asymptotic properties of fields and space-times. *Phys. Rev. Lett.*, 10:66–68, 1963.

[15] N.T. Bishop. Numerical relativity: combining the Cauchy and characteristic initial value problems. *Class. Quantum Grav.*, 10:333–341, 1993.

[16] C. Reisswig, N. T. Bishop, D. Pollney, and B. Szilagyi. Unambiguous determination of gravitational waveforms from binary black hole mergers. *Phys. Rev. Lett.*, 103:221101–1–221101–4, 2009.

[17] H. Friedrich and J.M. Stewart. Characteristic Initial Data and Wavefront Singularities in General Relativity. *Proc. R. Soc. London, Ser A*, 385:345–371, 1983.

[18] J. Winicour. Characteristic evolution and matching. *Living Rev. Relativity*, 12(3), 2009. `http://www.livingreviews.org/lrr-2009-3` (cited on 17 November 2009).

[19] C. Hellaby. The mass of the cosmos. *Mon. Not. R. Astron. Soc.*, 370:239244, 2006.

[20] K. Nakao C-M. Yoo, T. Kai. Solving the Inverse Problem with Inhomogeneous Universes. *Prog. Theor. Phys.*, 120:937–960, 2008.

[21] N.T. Bishop and P. Haines. Observational cosmology and numerical relativity. *Quaest. Math.*, 19:259–274, 1996.

[22] N.T. Bishop, R. Gomez, L. Lehner, M. Maharaj, and J. Winicour. High powered gravitational news. *Phys. Rev. D*, 56:6298–6309, 1997.

[23] H. Bondi. Gravitational waves in general relativity. *Nature*, 186:535–535, 1960.

[24] G.F.R Ellis. Relativistic Cosmology. In *General Relativity and Cosmology, Proc. Int. School of Physics 'Enrico Fermi' (Varenna), Course XLVII, Ed. R.K. Sachs*, pages 104–179. Academic Press, 1971. Reprinted in Gen. Rel. Grav. 41, 581 (2009).

[25] N.T. Bishop, R. Gomez, L. Lehner, M. Maharaj, and J. Winicour. Incorporating matter into characteristic numerical relativity. *Phys. Rev. D*, 60:024005–1–024005–11, 1999.

[26] R. L. Burden and J.D. Faires. *Numerical Analysis*. PWS Publishing Company Boston, fifth edition, 1993.

[27] G. Lemaître. l'Univers en expansion. *Annales de la Société Scientifique de Bruxelles*, A53(51), 1933. For an English transaltion see: The Expanding Universe. *Gen. Rel. Grav*, 29(5):641, 1997.

[28] R.C. Tolman. Effect of inhomogeneity on cosmological models. *Proc. Nat. Acad.*, Sci. 20:169, 1934.

[29] H. Bondi. Spherically symmetrical models in general relativity. *Mon. Not. Roy. Astr. Soc.*, 107:410, 1947. Also reprinted in: *Gen. Rel. Grav*, 31 (11):1783, 1999.

[30] G.F.R. Ellis and H. van Elst. Cosmological Models. *Cargèse Lectures*, 1998.

[31] J. Plebański and A. Krasiński. *An Introduction to General Relativity and Cosmology*. Cambridge University Press, first edition, 2006.

[32] J. Garcia-Bellido and T. Haugbølle. Confronting Lemaître-Tolman-Bondi models with observational cosmology. *JCAP*, 0804(003), 2008.
Also available at: `http://arxiv.org/abs/0802.1523`.

[33] M. N. Célérier and J. Schneider. A solution to the horizon problem: A delayed big bang singularity. *Phys. Lett. A*, 249:37–45, 1998.

[34] M. N. Célérier. Models of universe with an inhomogeneous big bang singularity III. Solving the horizon problem for an off-center observer. *A & A*, 362:840–844, 2000.

[35] J. Schneider and M. N. Célérier. Models of universe with an inhomogeneous big bang singularity II. CMBR dipole anisotropy as a byproduct of a conic big-bang singularity. *Phys. Lett. A*, 348:25–30, 1998.

[36] M. N. Célérier. Do we really see a cosmological constant in the supernovae data? *A & A*, 353:63, 2000.

[37] S. Perlmutter *et al.* Measurements of ω and λ from 42 high-redshift supernovae. *Astrophysical Journal*, 517(2):565–586, 1999.

[38] A.G. Riess *et al.* Observational evidence from supernovae for an accelerating universe and a cosmological constant. *Astronomical Journal*, 116:1009, 1998.
[39] K. Tomita. Distances and Lensing in Cosmological Void Models. *ApJ*, 529:38–46, 2000.
[40] J.E. Lidsey. ASTM108 Cosmology/MTH703U Advanced Cosmology. Lecturer's notes. `http://www.maths.qmul.ac.uk/~jel/ASTM108/#coursenotes` (cited: January 2010).